The spectral energy distributions of classical Cepheids in the Magellanic Clouds

Martin A.T. Groenewegen

Koninklijke Sterrenwacht van België, Belgium

The Introduction

Classical Cepheids (CCs) are an important standard candle because they are bright and provide a link between the distance scale in the nearby universe and that further out via those galaxies that contain both Cepheids and SNIa (see Riess et al. 2022 for a determination of the Hubble constant to 1.0 km s^{-1} precision). Typically, the period-luminosity (PL) relations of CCs that are at the core of the distance determinations are derived in particular photometric filters (V, I, K) or combination of filters that are designed to be reddening independent, the so-called Wesenheit functions (Madore 1982), e.g. using combinations of (V, I), (J, K), or the combination used by the SH0ES program (F555W, F814W, and F160W HST filters, see Riess et al. 2022).
On the other hand, the bolometric magnitude or luminosity is a fundamental quantity of CCs and stars in general as it is the output of stellar evolution models and the input to CC pulsation models. In Groenewegen (2020a, hereafter G20) the spectral energy distributions (SEDs) of 477 Galactic CCs were constructed and fitted with model atmospheres (and a dust component when required). For an adopted distance and reddening these fits resulted in a best-fitting bolometric luminosity (L) and the photometrically derived effective temperature ($T_{\rm eff}$). This allowed for the derivation of period-radius (PR) and PL relations, the construction of the Hertzsprung-Russell diagram (HRD), and a comparison to theoretical instability strips (ISs). The position of most stars in the HRD was consistent with theoretical predictions. Outliers were often associated with sources where the spectroscopically and photometrically determined effective temperatures differed, or with sources with large and uncertain reddenings.
This sample was further studied in Groenewegen (2020b), where the relation between bolometric absolute magnitude and the flux-weighted gravity (FWG), defined as $\log g_{\rm F} = \log g - 4 \cdot \log (T_{\rm eff}/10^4)$ (Kudritzki et al. 2003), was investigated: the so-called flux-weighted gravity-luminosity relation (FWGLR). The tight correlation between $g_{\rm F}$ and luminosity was first demonstrated by Kudritzki et al. (2003, 2008) for blue supergiants, and was then used for extra galactic distance determinations in Kudritzki et al. (2016). Anderson et al. (2016) then demonstrated that theoretical pulsation models for CCs also followed a tight FWGLR, in fact tighter than the PL relation, and that there was a good correspondence between observed $g_{\rm F}$ and period for a sample of CCs. Groenewegen (2020b) presented the best observationally determined FWGLR, based on the luminosities derived in G20 and gravity and effective temperatures from the literature.
The advantage of using the Magellanic Clouds is that accurate and independently derived mean distances are available based on the analysis of samples of eclipsing binaries (Pietrzynski et al. 2019, Graczyk et al. 2020).
The present study performs a study similar to G20 and Groenewegen (2020b) for a sample of CCs in the small (SMC) and large Magellanic cloud (LMC).
This poster presents preliminary results; a paper describing this research in detail is in preparation.

The Sample

In this paper a sample of 139 LMC and 61 SMC are studied. Although this is a small subset of the about 4700 LMC and 4900 SMC CCs known in the MCs (see e.g. Ripepi et al. 2017, Ripepi et al. 2022a) the stars in this sample are of special interest as they have been studied in other respects. In particular the sample is composed of

- Eighty-nine LMC CCs for which Romaniello et al. (2022) derived iron and oxygen abundances (as well as effective temperatures and gravities) from high-resolution spectroscopy. This sample is composed of 68 CCs used to define the PL-relation in the LMC in the SH0ES program (Riess et al. 2019) and 21 for which archival spectra, first presented in Romaniello et al. (2008), were re-analysed.
- Fourteen SMC CCs for which Romaniello et al. (2008) performed an abundance analysis. Note that for the LMC CCs in overlap Romaniello et al. (2022) derived an iron abundance that was on average 0.1 dex smaller compared to Romaniello et al. (2008).
- CCs for which a Baade-Wesselink analysis has been carried out, in particular the 36 LMC and five SMC stars considered in Storm et al. (2011), and the essentially identical sample of 36 LMC and six SMC stars considered in Groenewegen (2013).
- CCs for which light-curves (and sometimes radial-velocity curves) have been fitted with theoretical pulsation models. In such modelling (Marconi et al. 2013) the stellar mass, luminosity, (mean) effective temperature are derived by fitting light-curves (typical V, I and K). The apparent distance moduli (DM) are derived from which the true DM and reddening are found. If RV curves are fitted, the projection-factor (p-factor) is also derived. Considered are the 11 LMC and 9 SMC fundamental-mode (FM) CCs studied in Ragosta et al. (2019) and Marconi et al. (2017), respectively.
- CCs with (previously unpublished) photometry in the Walraven system. This system is very useful in constraining effective temperature and reddening as the photometric bands extend into the blue. van Genderen (1983) published VBLUW photometry for 21 SMC and 20 LMC CCs using data taken between 1971 and 1978. However, data taking continued after that from ESO Chile, and these observations will be published.
- CCs in the MCs with RV curves published in *Gaia* DR3 (Gaia collaboration 2022, Ripepi et al. 2022b). These objects may be of interest in future BW studies.
- SMC FM CCs for which UVES spectra (M. Romaniello, private communication) and in part *HST* photometry (A. Riess, private communication) will be obtained in the near future.

There are stars in overlap between the different subsamples, and the final sample consists of 139 LMC and 61 SMC CCs, all FM pulsators.
The spectral energy distributions (SEDs) are constructed using photometry retrieved mostly, but not exclusively, via the VizieR web-interface. This includes GALEX, various OGLE catalogues (including Soszynski et al. 2017), Gaia DR3 photometry, Skymapper DR2 (Onken et al. 2019), *HST* F555W, F814W, and F160W photometry from Riess et al. (2019) for the LMC, infrared data from the VMC (Cioni et al. 2011, Ripepi et al. 2016, Ripepi et al. 20221), Persson et al. (2004), Macri et al. (2015), Akari (Ita et al. 2010, Kato et al. 2012), AllWISE (Cutri 2013), IRAC (Chown et al. 2021), and Walraven and older UBV photometry from various sources.

The Modelling

The SEDs are fitted with the code More of DUSTY (MoD, Groenewegen (2012) which uses a slightly updated and modified version of the DUSTY dust radiative transfer (RT) code (Ivezic et al. 1999) as a subroutine within a minimisation code. As we are not interested here in any dust component (in fact, all SEDs are consistent with no dust being present), the dust optical depth is set to zero. In that case the input to the model are the distance, reddening, and a model atmosphere.
The advantage of using the Magellanic Clouds is that accurate and independently derived mean distances are available based on the analysis of samples of eclipsing binaries (Pietrzynski et al. 2019, Graczyk et al. 2020). The mean distance to the LMC is adopted to be $d_{\rm LMC} = 49.59 \pm 0.09$ (**stat**) ± 0.54 (syst) kpc (Pietrzynski et al. 2019), and to the SMC of $d_{\rm SMC} = 62.44 \pm 0.47$ (**stat.**) ± 0.81 (syst.) kpc (Graczyk et al. 2020), based in both cases on the analysis of samples of eclipsing binaries. The depth effect in the SMC is considerable, e.g. Ripepi et al. (2017), but all SMC sources have been adopted to be at the mean distance. For the LMC the first order approximation of an inclined disk is adopted to compute the geometric correction, and the procedure in Riess et al. (2019) is followed, taking the inclination and position angle of the line of nodes of the disk from Pietrzynski et al. (2019) and the LMC center-of-mass coordinates from van der Marel & Kallivayalil (2014).
The model atmosphere fluxes are reddened to be compared to the observations. The reddening map of Skowron et al. (2021) for the MCs is adopted and the $E(V-I)$ value in the map closest to the source is taken. The visual extinction is then assumed to be $A_{\rm V} = E(V-I)/1.318 \cdot 3.1$.
MARCS model atmospheres are used as input (Gustafsson et al. 2008) for log g = 1.5 and metallicity -0.50 and -0.75 dex for the LMC and SMC stars, respectively. For every model atmosphere (that is, effective temperature) a best-fitting luminosity (with its [internal] error bar, based on the covariance matrix) is derived with the corresponding reduced chi-squared of the fit. The model with the lowest $\chi^2_{\rm r}$ then gives the best-fitting effective temperature. Considering models within a certain range above this minimum $\chi^2_{\rm r}$ then gives the estimated error in the effective temperature and luminosity. For the luminosity this error is added in quadrature to the internal error in luminosity.
Figure 1 below shows some the fits that can be obtained.

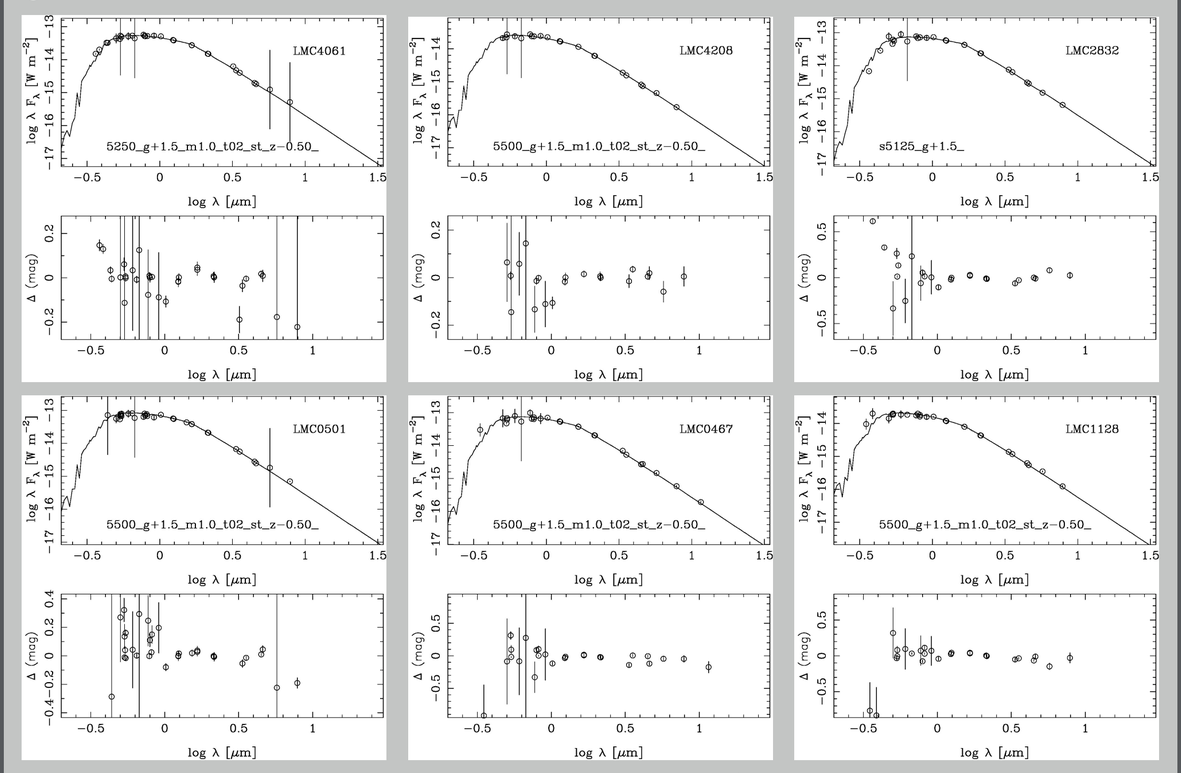

Figure 1: Examples of fits to the SEDs. The upper panels show the observations (with error bars) and the model. The lower panel shows the residuals. Outliers have been plotted with an (arbitrary) error bar of 3.0 mag.

The Results

Figure 2 shows the HRD together with sets of evolutionary tracks and ISs, see a detailed explanation in the caption regarding the meaning of the symbols, colours, and lines. Overall there is a very good agreement between the position of the CCs in the sample and the theoretical instability strips, with only two clear outliers (why this could be the case is under investigation). The HRD also includes the position of the six known CCs in eclipsing binaries as blue points (from Pilecki et al. 2018). They seem to be too hot for the ISs calculated by De Somma et al. (2021) but agree with the ISs calculated by Pilecki et al. themselves.

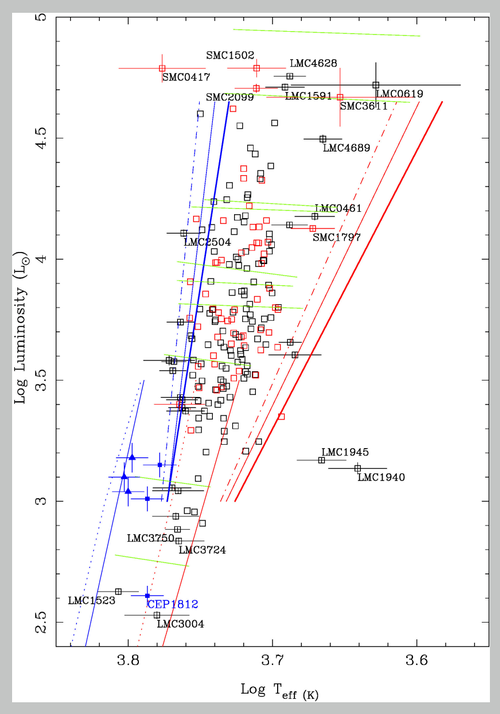

Figure 2. The Hertzsprung-Russell diagram. Black and red open squares indicate LMC and SMC CCs from the sample, respectively. Stars located outside the bulk of objects are plotted with error bars, and some are labelled as well. Blue symbols with error bars indicate the location of the 6 known CCs in EBs (three FM as filled squares, three FO as filled triangles, from Pilecki et al. 2018). Blue and red lines indicate the blue and red edge of the IS. In the upper part (brighter than $\log L = 3$) the results from De Somma et al. (2021) are plotted. The thinner solid and dot-dashed line are for $Z = 0.008$ and $Z = 0.004$ models, respectively, for their type A mass-luminosity relation. The tick line is for $Z = 0.008$ for their type-B mass-luminosity relation. In the lower part (fainter than $\log L = 3.5$) results from Pilecki et al. (2018) are plotted for FM (solid lines) and FO (dotted lines) model. Green lines indicate evolutionary models from Anderson et al. (2016). Increasing in luminosity are tracks for initial mass (number of the crossing through the IS): 4 (1), 5 (1), 7 (1), 7 (2), 7 (3), 9 (1), 9 (2), 9 (3), 12 (1), 15 $M_\odot$(1).

Figure 3 shows the relation between $M_{\rm bol}$ and $\log R$ with log Period.
Preliminary fits to the entire sample are

$$M_{\rm bol} = (-3.01 \pm 0.05) \log P + (-1.07 \pm 0.06) \quad (1)$$

with an rms of 0.24 mag, and

$$\log R = (0.6953 \pm 0.0047) \log P + (1.1200 \pm 0.0055), \quad (2)$$

with an rms of 0.019 dex.
What is interesting too not is that the six known CCs in EBs agree perfectly with the PR relation derived for the entire sample, but are brighter than the mean PL relation for the sample. The radius is a direct derivation from the light curve and radial velocity analysis of EBs, but the luminosity is derived via the effective temperature. As the temperatures also seemed to be hotter than the photometric temperatures derived for the sample stars at similar luminosities, the two effects may be related (and this is under further investigation).

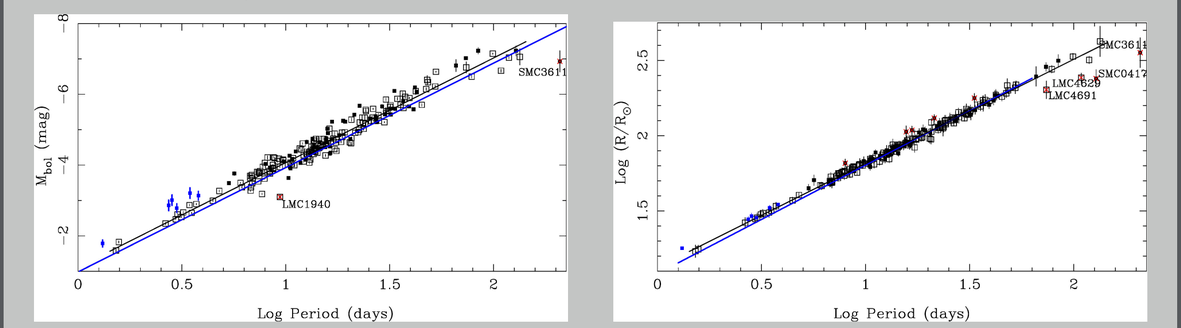

Figure 3: The left-hand panel shows the period-$M_{\rm bol}$ relation. Outliers are identified. The black line indicates the best fit to the sample (see text). The blue line gives the PL relation for Milky Way (MW) CCs from Groenewegen et al. (2020a). The right-hand panel shows the period-radius relation. Some outlying stars are identified. The black line indicates the best fit to the sample (see text). The blue line gives the PR relation for MW CCs from Groenewegen et al. (2020a).

The mass-luminosity relation

The luminosities are derived in an independent may, and we have an estimate for the mass, the mass-luminosity relation can be investigated.
Five different mass estimates have been used:

- The period-luminosity-mass-effective temperature-metallicity relation derived in Groenewegen & Jurkovic (2017) based on the models of Bono et al. (2001).
- A similar relation has been derived based on the models of Anderson et al. (2016).
- The period-mass-radius relation based on the model fitting of LMC Cepheid light curves from Ragosta et al. (2019).
- The period-mass-radius relation derived in Pilecki et al. (2018) from the analysis of the light- and radial-velocity curves of the 6 known CCs containing EB systems.
- The period-mass-*Gaia*-based Wesenheit relation from Marconi et al. (2020) based on nonlinear convective pulsation models

The adopted mass is the median among the five estimates. To estimate the error bar, the error in the mass estimate of the median value is added in quadrature to the median-absolute-deviation times 1.48 (to get the equivalent of one sigma in a Gaussian distribution) among the 5 estimates. The mass-luminosity relation is shown in Figure 4.

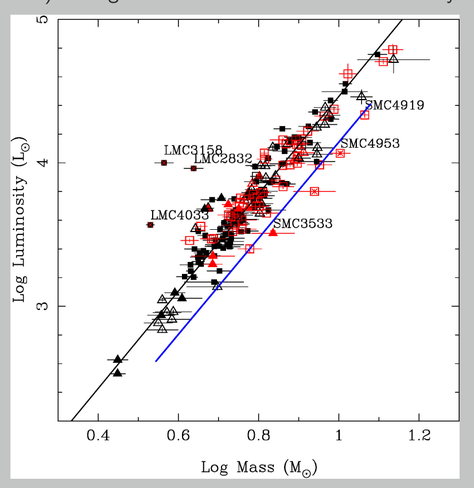

Figure 4. The mass-luminosity relation. Objects in the SMC are plotted in red. Stars outside the bulk of objects are identified. The blue line indicates the canonical ML relation from Bono et al. (2000b) for Y=0.255 and Z=0.008. For Z=0.004 the line would be at higher luminosities by 0.1 dex . The black line indicates a fit to the LMC stars minus the three marked by a red cross and lies almost exactly +0.3 dex above the canonical ML relation

A **Preliminary** fit to the data is

$$\log L = (3.392 \pm 0.078) \log M + (1.071 \pm 0.060) \quad (3)$$

and lies about +0.3 dex above the canonical relation in Bono et al. (2000b), and is the intermediate between the case-B (+0.2 dex) and case-C (+0.4 dex) ML-relations adopted in Marconi et al. (2020).

The References

- Anderson, Saio, Ekström, et al. 2016, A&A 591, A8
- Bono, Castellani, & Marconi, 2000a, ApJ 529, 293
- Bono, Caputo, Cassisi, S., et al. 2000b, ApJ 543, 955
- Chown, Scowcroft, & Wuyts, 2021, MNRAS 500, 817
- Cioni, Clementini, Girardi, et al. 2011, A&A 527, A116
- Cutri, 2013, VizieR Online Data Catalog: AllWISE Data Release
- De Somma, Marconi, Cassisi, et al. 2021, MNRAS 508, 1473
- Gaia Collaboration, Vallenari, Brown, Prusti, et al. 2022, arXiv;220800211G
- Graczyk, Pietrzynnski, Thompson, et al. 2020, ApJ 904, 13
- Groenewegen 2012, A&A, 543 A36
- Groenewegen 2013, A&A 550 A70
- Groenewegen 2018, A&A 619, A8
- Groenewegen 2020a, A&A 635, A33
- Groenewegen 2020b, A&A 640, A113
- Groenewegen & Jurkovic, 2017, A&A 604, A29
- Gustafsson, Edvardsson, Eriksson, et al. 2008, A&A 486, 951
- Ita, Onaka, Tanabé, et al. 2010, PASJ 62, 273
- Ivezic, Nenkova, & Elitzur, M. 1999, DUSTY: Radiation transport in a dusty environment, Astrophysics Source Code Library
- Kato, Ita, Onaka, et al. 2012, AJ 144, 179
- Kudritzki, Bresolin, & Przybilla 2003, ApJ 582, L83
- Kudritzki, Urbaneja, Bresolin, et al. 2008, ApJ 681, 269
- Kudritzki, Castro, Urbaneja, et al. 2016, ApJ 829, 70
- Macri, Ngeow, Kanbur, Mahzooni, & Smitka 2015, AJ 149, 117
- Madore, 1982, ApJ 253, 575
- Marconi, Molinaro, Ripepi, Musella, & Brocato, 2013, MNRAS 428, 2185
- Marconi, Molinaro, Ripepi, et al. 2017, MNRAS 466, 3206
- Marconi, De Somma, Ripepi, et al. 2020, ApJ 898, L7
- Onken, Wolf, Bessell, et al. 2019, PASA 36, e033
- Persson, Madore, Krzeminìski, et al. 2004, AJ, 128 2239
- Pietrzynski, Graczyk, Gallenne, et al. 2019, Nature 567, 200
- Pilecki, Gieren, Pietrzynìski, et al. 2018, ApJ 862, 43
- Ragosta, Marconi, Molinaro, et al. 2019, MNRAS 490, 4975
- Riess, Casertano, Yuan, Macri, & Scolnic, D. 2019, ApJ 876, 85
- Riess, Yuan, Macri, et al. 2022, ApJ 934, L7
- Ripepi, Marconi, Moretti, et al. 2016, ApJS 224, 21
- Ripepi, Cioni, Moretti, et al. 2017, MNRAS 472, 808
- Ripepi, Chemin, Molinaro, et al. 2022a, MNRAS 512, 653
- Ripepi, Clementini, Molinaro, et al. 2022b, arXiv:2206.06212
- Romaniello, Riess, Mancino, et al. 2022, A&A 658, A29
- Romaniello, Primas, Mottini, et al. 2008, A&A 488, 731
- Soszynski, Udalski, SzymanÃÂski, et al. 2017, Acta Astron. 67, 103
- Skowron, Skowron, Udalski, et al. 2021, ApJS 252, 23
- Storm, Gieren, Fouqué, et al. 2011, A&A 534, A95
- van der Marel & Kallivayalil 2014, ApJ 781, 121
- van Genderen 1983, A&AS 52, 423

martin.groenewegen@oma.be